Zhiyuan Chen, Lijun Wang*, Ziyou Yu, Fushen Li, Zaihong Sun, Hailei Zhao and Kuo Chih Chou

Corrosion Process of Stainless Steel 441 with Heated Steam at 1,000 °C

DOI 10.1515/htmp-2015-0238
Received October 24, 2015; accepted May 31, 2016

Abstract: Stainless steel 441 was oxidized in water vapor containing atmospheres at 1,000 °C to study the contrary effects of water vapor on the oxidization process. The steel in 3.5 vol. % H_2O containing atmosphere exhibited an relatively strong protective behavior. The reason was that the densification of the chromium oxide scale was promoted due to the sintering of the oxide grains via Cr-containing species vapor. But the oxidation of the steel in 11.5 ~ 15.6 vol. % H_2O containing atmosphere followed a non-protective breakaway oxidation due to the breakage of the dense scale by "bubbles" and the formation of iron-rich oxides layer. Experimental result shows that the growth stress increased about 2 GPa during the first 70 ks in wet oxidizing atmosphere. The relatively slow increase of the oxides scale growth stress could be release in water vapor containing atmosphere.

Keywords: solid oxide fuel cell, interconnect, steam, Fe-Cr alloys, high temperature oxidation, Raman spectrum

PACS® (2010). 64.75.Lm

Introduction

Stainless steel has been widely applied in high-temperature environments containing water vapor, such as heat exchangers in power plants, boiler components and interconnectors in solid oxide fuel cells [1–7]. As it is well known, the oxidation performance of stainless steel mainly depends on the potential to form and maintain a Cr-rich protective oxide scale. However, in the presence of water vapor, the changes in the structure and performance of the protective oxide scale must be reconsidered, since many investigations have proved that water vapor could influence the high temperature oxidation process of stainless steel [7, 8]. The effects of water vapor on the oxidation of alloy, especially on stainless steel can be divided into:

(1) Water vapor could increase the adherence of oxide scales [9, 10];
(2) It could promote the internal oxidation of Cr-based alloy [11];
(3) The conductivity of the formed scale could be increased in water vapor containing atmosphere [9];
(4) The oxidation rate of stainless steel could be promoted by introducing water vapor in the atmosphere [11–15].

Essuman et al. [11] and Othman et al. [13] summarized the oxidation mechanisms of alloy in water vapor containing atmospheres. One of the important mechanisms is that water can modify the diffusion mode of oxygen in the oxide scale [16, 17]. This is because of the internal oxidation of metal under the oxide scale. Another important problem with respect to the oxidation of stainless steel in oxidizing atmospheres is Cr evaporation, especially in water vapor containing atmosphere. The analysis of the Cr-vapor species was also widely reported [18–22].

However, the oxidizing rate of stainless steel in low water vapor containing oxidizing atmosphere has not been widely examined in literature. Even the conclusions earlier reported are contradictory to many reports [10, 11, 23]. In the present work, the corrosion kinetics of the stainless steel 441, one of the typical materials using at high temperature, was studied by thermogravimetry in dry and wet air. The oxidation process and its mechanism of the stainless steel 441 in wet air are discussed.

Experimental section

The investigated stainless steel 441 was supplied by HuaTsing Power Sci&tech Co. The chemical compositions

***Corresponding author: Lijun Wang,** Collaborative Innovation Center of Steel Technology, University of Science and Technology Beijing, Beijing, 100083, CHINA, E-mail: lijunwang@ustb.edu.cn
Zhiyuan Chen, School of Materials Science and Engineering, University of Science and Technology Beijing, Beijing, 100083, PR CHINA
Ziyou Yu, State Key Laboratory of Advanced Metallurgy, University of Science and Technology Beijing, Beijing 100083, PR CHINA
Fushen Li, School of Materials Science and Engineering, University of Science and Technology Beijing, Beijing, 100083, PR CHINA
Zaihong Sun, Suzhou HuaTsing Power Sci. & Tech. Co., Ltd., Kunshan 215313, PR China
Hailei Zhao, School of Materials Science and Engineering, University of Science and Technology Beijing, Beijing, 100083, PR CHINA
Kuo Chih Chou, State Key Laboratory of Advanced Metallurgy, University of Science and Technology Beijing, Beijing 100083, PR CHINA

Table 1: The chemical compositions of the stainless steel 441.

Composition	Fe	Cr	C	Mn	Nb	Ti	Si	P	S
Mass%	80.6	18.3	0.008	0.2	0.5	0.2	0.3	0.022	0.002

are shown in Table 1. The main elements were rechecked by the China National Center for Quality Supervision and Testing of Iron and Steel. The steel specimens, cut into sheets of $0.7 \times 20 \times 40$ mm with specular gloss, were cleaned in alcohol, and dried before oxidation treatment. A small hole (diameter is 2 mm) was drilled in the upper part of the alloy so that a thin alumina rod could be inserted for hanging the specimen in the thermoanalyzer.

The specimens were oxidized at 1,000 °C for 8.3 h in air with high water vapor contents (>10 %) and 13.9 h with low water vapor contents (<10 %), respectively. This temperature is within a common oxidation test temperature range of 18 wt%-Cr-containing steel. Mass changes of the specimens during the oxidation process were recorded by the balance to an accuracy of 0.1 mg (made by Shanghai Youke instrument Co. Ltd.). Figure 1 shows the device which connects the specimen to the balance. The gas flow was maintained at 100 ml/min STP (accuracy ±1.8 ml/min) by means of an Alicat Gas Flow Controller. And liquid water was pumped into a steam generator (temperature was kept at 300 °C) using a MasterFlex peristaltic pump (accuracy ±0.1 %). Water vapor and air were mixed in the generator, and then fed into the furnace.

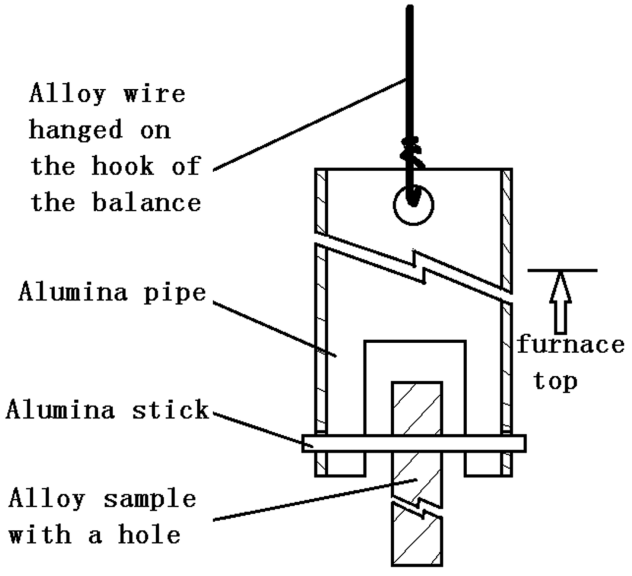

Figure 1: Device of connecting alloy sample to the balance in the oxidation treatment.

A scanning electron microscope (SEM, CARL ZEISS EVO MA 10/LS 10 JS) with energy dispersive spectrum (EDS, Thermo NORAN System) was employed to probe the topography of the specimens after oxidation. Raman spectrum (Horyba LabRAM HR Evolution) was also applied to investigate the component and growth stress of the oxidized specimens. The sample surface was probed with a 100 μm-spot-sized laser (532 nm laser in 25 mW).

Results and discussion

Mass-change of the specimens

Figure 2(a) is the mass-change profiles of the stainless steel 441 in wet atmosphere at 1,000 °C. The mass-change is expressed as $\Delta m/S$, where Δm is the mass gain of the specimen, and S is the exposure area of the specimen. The initial oxidation rate of the specimen was relatively fast in the air with low water vapor content (0 vol. % and 3.5 vol. % H_2O). Usually, the mass gain profiles followed a quasi-parabolic rule. When the water vapor content was elevated to no less than 11.5 vol. %, the initial oxidation rate was lower. However, the oxidation slightly accelerated with the prolonged exposure time. It was due to the non-protective oxides scale and evaporation of Fe and Cr bearing substances, which will be introduced later. The oxidation kinetic profiles of Fe-Cr alloys in H_2O containing atmosphere [11, 13] also showed the similar breakaway process. This process is usually described as following equation,

$$t = \frac{k_d}{k_s^2}\left[-\frac{k_s}{k_d}\frac{\Delta m}{A} - \ln\left(1 - \frac{k_s}{k_d}\frac{\Delta m}{A}\right)\right] \quad (1)$$

where Δm is the sample weight change, A is the sample surface area, t is the oxidation time. The two constants, k_d and k_s, describe the diffusion process within the oxidized steel and Cr evaporation in the oxidation, respectively. Equation (1) indicates that the initial mass gain rate of alloy in moist high temperature atmosphere is the Highest during the process, and then it will decrease to a stable value. It can be noticed that the oxidation process of steel in dry atmosphere can be perfectly described by this model, where $k_d = 2.09 \times 10^{-5}$ mg·cm^{-2}·s^{-1} and $k_s = 4.51 \times 10^{-6}$ mg·cm^{-2}·s^{-1}.

The oxidation of steel in moist atmosphere did not follow the quasi-parabolic mechanism. Further, the oxidation rate tended to be constant without any noticeable increase with prolonged exposure. In this situation, the process could be approximately treated as a simplified

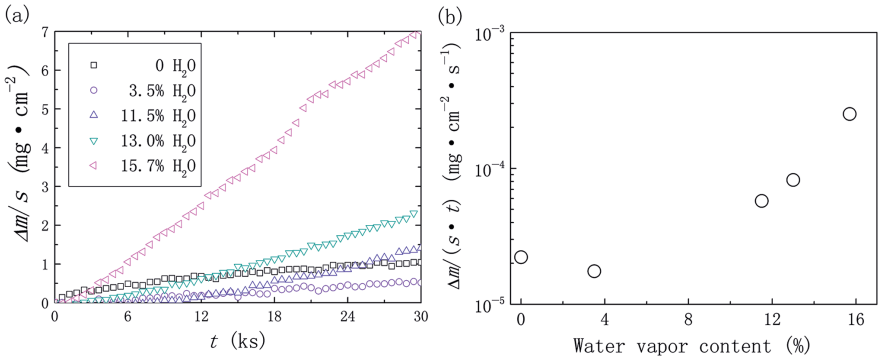

Figure 2: (a) Mass-change profiles and (b) absolute value of k_s of stainless steel 441 in wet air at 1,000 °C.

pattern of eq. (1): k_d is assumed to be a relatively large number comparing to k_s, in which it is implied that the protection of oxides scale is not such effective. It results in the eq. (1) to be

$$t = -\frac{1}{k}\frac{\Delta m}{A} \tag{2}$$

where the physical meaning of k changes to be apparent reaction rate constant. Values of k of the mass-change profiles of the samples in various atmospheres were worked out for comparison. Considering the comparability, mass–gain curve in dry air was also fitted by eq. (2). Figure 2(b) shows that the absolute value of k decreased firstly, and then increased exponentially with increasing water vapor content in the atmosphere. Wet air with 3.5 vol. % H_2O and dry air were beneficial to the oxidation resistance of stainless steel 441, which had the lowest average oxidation rate.

Topography of the oxide scale

With the increase of the water vapor content in the atmosphere, the topography of the oxide scale varied. Magnification views of the near surface region are shown in Figure 3. The oxide grains were fine in low water vapor-containing atmospheres. The grains sintered more seriously with the increase of water vapor content. When the water vapor content was as high as 11.5 vol. %, the oxide grains were compacted fully due to sintering. A large number of small "bubbles" and broken ones were found spreading all over the scale surface. The "bubbles" on the surface implied the formation of vapor molecules under the dense scale in the oxidation.

Big "bubbles" were found on the scale which developed in high water vapor containing atmospheres (Figure 4). The similar phenomenon has earlier been reported [24–26]. Surface of the "bubbles" was porous.

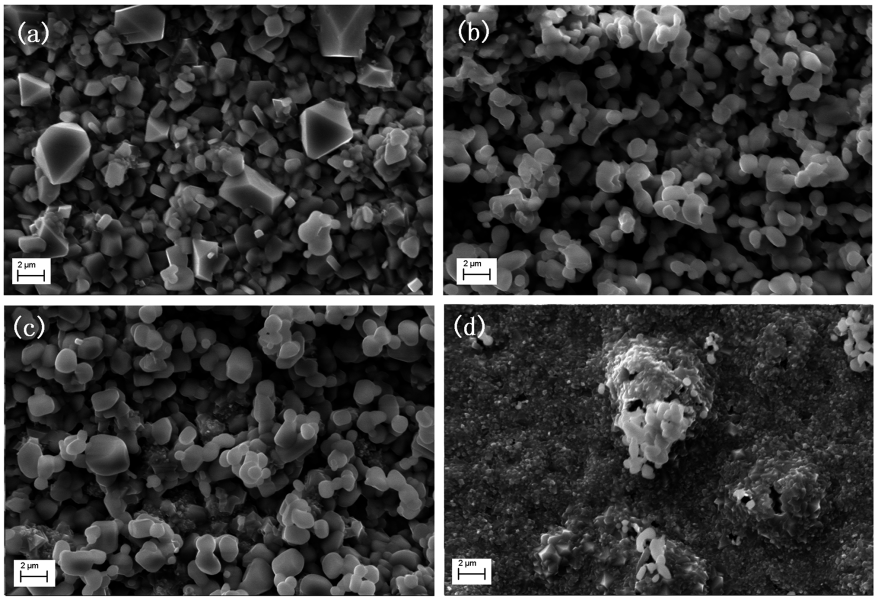

Figure 3: Surface morphology of scale surfaces developed on stainless steel 441 at 1,000 °C in (a) dry air, (b) air with 3.5 vol. % H_2O, (c) air with 8.2 vol. % H_2O, (d) air with 11.5 vol. % H_2O.

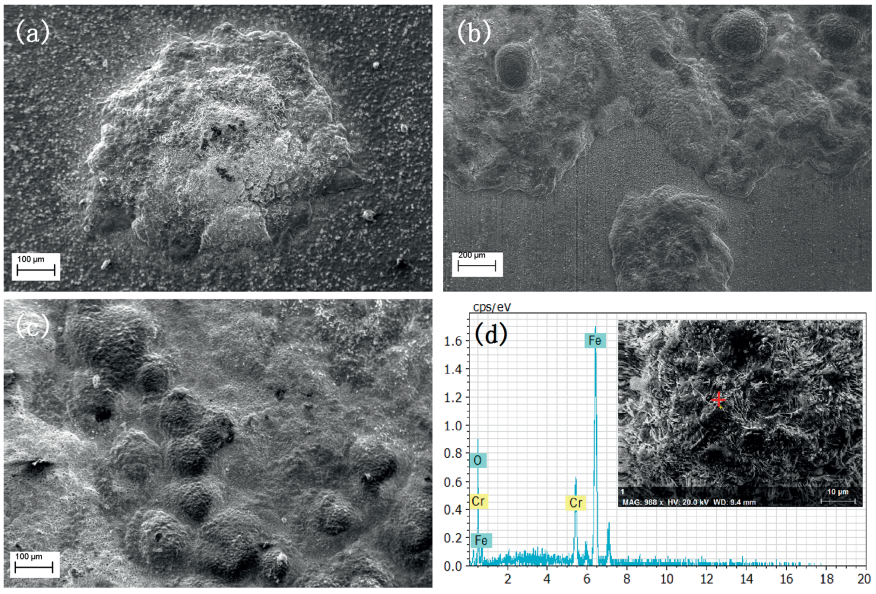

Figure 4: Surface morphology of big "bubbles" on the scale surfaces developed on stainless steel 441 at 1,000 °C in air with (a) 11.5 vol. % H_2O, (b) 13.0 vol. % H_2O, (c) 15.7 vol. % H_2O, (d) EDS of blade-like Fe_2O_3 grains on the surface of the bubbles.

Fe_2O_3 grains in the shape of blades were found on the surface of the "bubbles" (Figure 4(d)). The diameters of the "bubbles" were about ten to hundreds of micrometers. The "bubbles" expanded and were connected to each other with the increase of time and water vapor content. EDS investigations revealed that these consisted of (Fe,Cr) spinel and Fe_2O_3. Total covered area of the Fe-rich "bubbles" on the Cr_2O_3 scale was larger in air with higher water vapor content.

The oxides in the broken "bubbles" were analyzed. Figure 5 shows that the region was composed of Fe-rich oxides. It implied that a serious oxidization occurred on the broken zone in wet air for the non-protective from oxides scale.

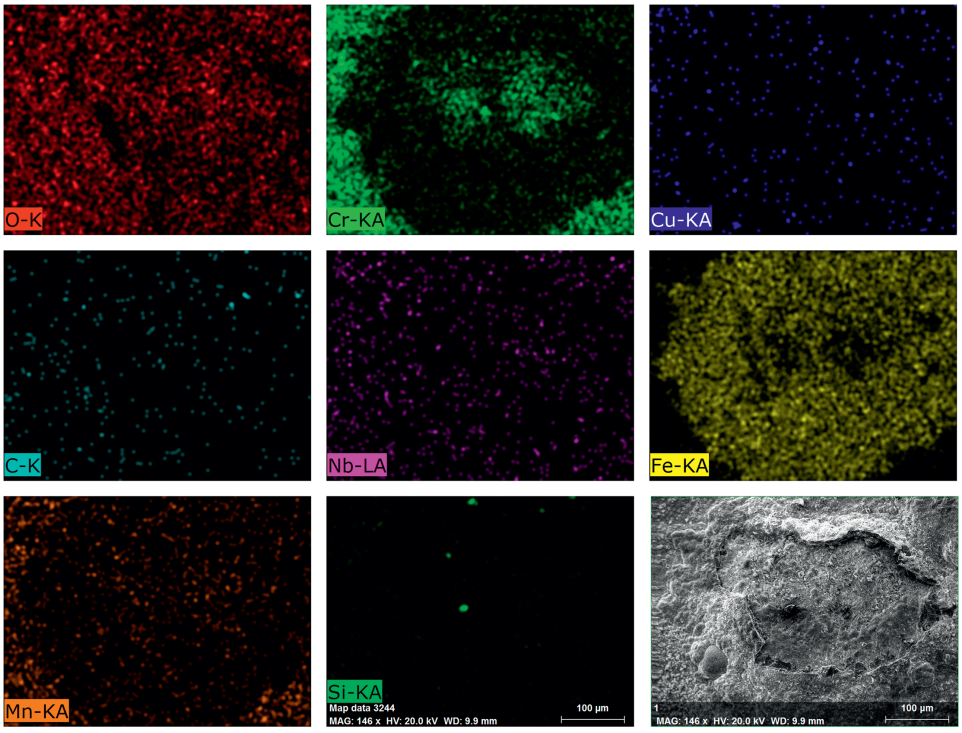

Figure 5: EDS map of the broken oxide scale and the internal oxides which developed at 1,000 °C in air with 11.5 vol. % H_2O.

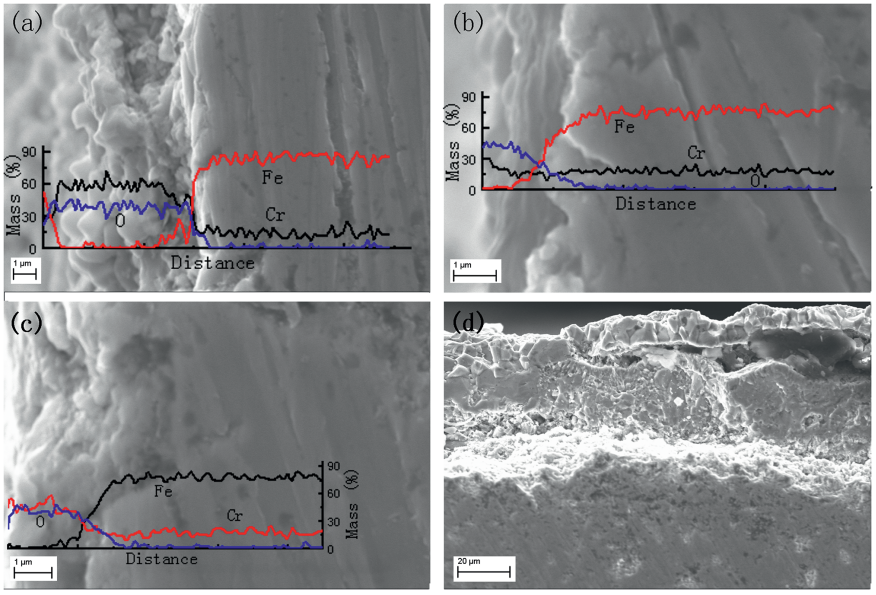

Figure 6: SEM image and element distribution probed by EDS for the oxidized stainless steel at 1,000 °C in (a) dry air; (b) air with 3.5 vol. % H_2O; (c) air with 11.5 vol. % H_2O (Cr_2O_3 based scale); (d) air with 11.5 vol. % H_2O (Fe-rich oxides scale).

The cross section of the oxidized stainless steel was shown in Figure 6. EDS results showed that the oxide layer contained mainly Cr and O. The thickness of the scales in dry air is about 4 μm, which is thicker than the scale thickness (1 μm) in wet air containing 3.5 vol. % water vapor. It indicated that the oxidation rate of the stainless steel 441 in wet air (3.5 vol. % H_2O) was relatively slow. And the increased Fe content on the surface of oxide layer in Figure 6(a) also indicated that the oxidation of stainless steel 441 in dry air was more serious than it in air with 3.5 vol. % H_2O. Oxides scales developed in wet air with more than 10 vol. % H_2O shows two different cross sections. Figure 6(c) shows the most part of stainless steel 441 was covered with Cr_2O_3 based dense scale, which was determined by EDS. While Figure 6(d) shows that thick scale with Fe-rich oxides formed at some part. As mentioned, it was a part of expanded Fe-rich "bubble". EDS results indicated that the oxides in Figure 6(d) from the surface of scale to the interface of oxides/steel were iron oxides, $(Fe,Cr)_3O_4$ and Cr_2O_3 in sequence.

Oxidation process

Figure 7 shows the topography of the scale in wet air at 1,000 °C with different oxidation times. The scale which initially formed in 11.5 vol. % H_2O containing air was dense and the boundaries of the grains were identifiable. With the exposure time increasing, some Cr_2O_3 fine grains developed from the dense Cr_2O_3 scale, and then sintered to be a uniform scale (Figure 3(d)).

The specimens were also analyzed by Raman spectra to confirm the oxidation products in two different stages, as shown in Figure 8. The bands around 225, 498 (A_{1g} modes), 247, 293, 299, 412 and 613 cm^{-1} (E_g modes) were attributed to hematite [27]. The Raman bands of Cr_2O_3

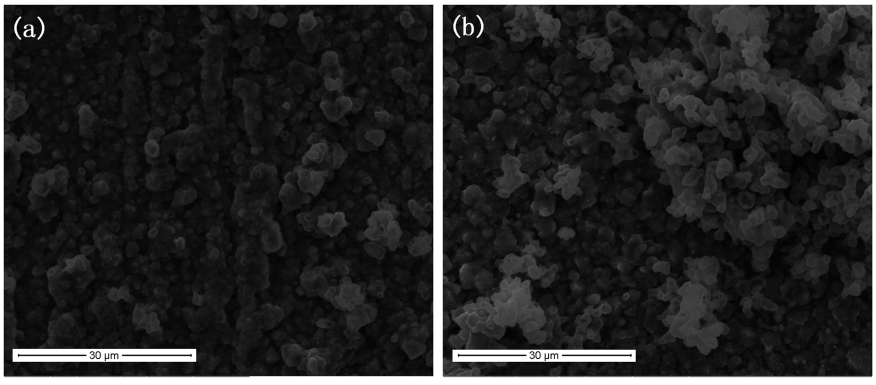

Figure 7: Surface morphology of scale surfaces developed on stainless steel 441 at 1,000 °C in air with 11.5 vol. % H_2O in (a) 2 h, (b) 5 h.

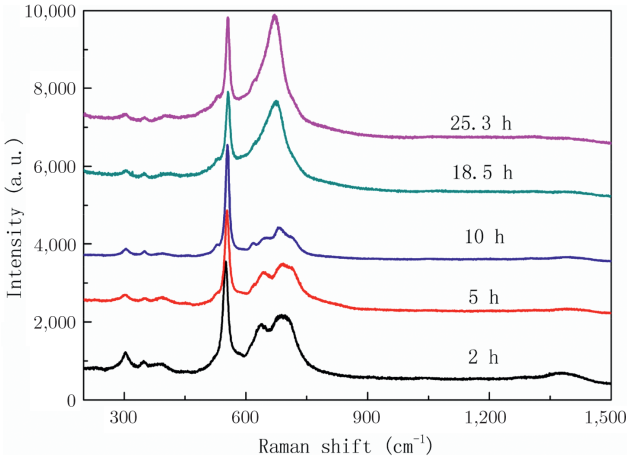

Figure 8: Raman spectra of stainless steel 441 oxidized for different times at 1,000 °C in air with 11.5 vol. % H_2O.

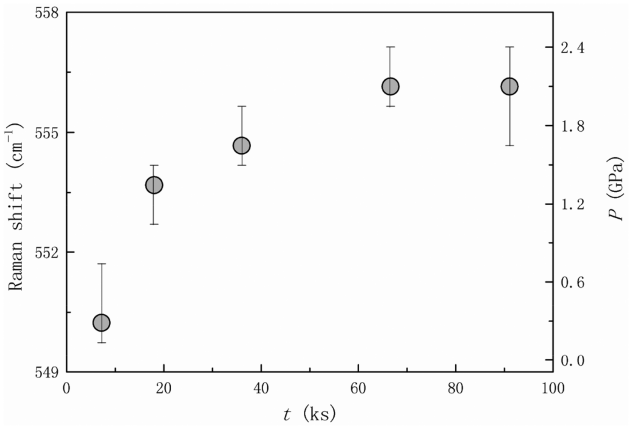

Figure 9: Raman band shift and growth stress of Cr_2O_3 in the scales which developed on stainless steel 441 for different times at 1,000 °C in air with 11.5 vol. % H_2O.

were around 235, 296.3, 350.4, 528.5, 615.0 (E_g modes), 266 and 554.2 cm^{-1} (A_{1g} modes) [28, 29]. Bands around 664–685 cm^{-1} and 680–690 cm^{-1} were attributed to corundum solid solution and spinel phases respectively [30]. The relative intensity of the band around 680–690 cm^{-1} (spinel phases) increased with the increase of exposure time. Meanwhile, the relative intensity of the band around 554.2 cm^{-1} (Cr_2O_3) decreased. It implied that the content of Cr_2O_3 was lower and the content of Fe-containing spinel phases was higher in the oxide layers when the exposure time was prolonged. Thus, the oxidation resistance of the oxide layer was weakening with the increased time in the oxidation process. But the main composition of the oxide layers was still Cr_2O_3 within 90 ks.

The Raman shift of the strongest band of Cr_2O_3 (554.2 cm^{-1}) was recorded (as shown in Figure 9). The shifts of Raman bands were mainly due to the growth stress in the oxidation process [31]. So the Raman shift of the band could be used to explore the growth stress of the oxidation process [29, 32]. The relaxed oxide growth on the stainless steel was reported at 549.3 cm^{-1} [32]. Figure 8 shows that the Raman shift of the band increases with the increasing exposure time in a parabolic-like relationship. The band shift was not obvious after more than 60 ks of oxidation in wet air. The stresses were calculated by the equation in Ref. [28, 29, 32]:

$$\Delta\nu/\mathrm{cm}^{-1} = 3.26 \times P/\mathrm{GPa} \quad (3)$$

where $\Delta\nu$ is the band shift to the reference wavenumber 549.3 cm^{-1}, P is the growth stress of the scale. Thus, the influence of exposure time on the growth stress of the oxide scales could also be expressed as a parabolic-like relationship, which is similar to the oxidation process of 441 in dry oxygen. In the oxidation of Fe-18Cr-TiNb alloy, the growth stress of the scale increases quickly to around 2 GPa at about 3 ks, then decreases very slowly [32]. But the growth stress of scale in wet air was found to increase within about 70 ks, which was much longer than the one in the dry oxygen. The slower increase of the growth stress implied that the stress caused by volume expansion of the formed oxide was getting relaxed. There might be two reasons for the relaxation. Firstly, the relative serious internal oxidation of the alloy eased the epitaxial stress of the oxide scales and the metal. Secondly, the formation and breakage of "bubbles" released part of the growth stress.

Mechanism analysis

The oxidation acceleration of alloy in high water vapor containing atmosphere was reported by many earlier workers [10, 11, 23, 33]. However, it was concluded that the effects of water vapor on the stainless steel oxidation were complex, without a specific conclusion as to whether it could be beneficial or detrimental [34]. The complex effects of water vapor could lead to various results in practice. The oxidation kinetics of the alloy at high temperature always could be quasi-parabolic or linear. In our study, the oxidation of stainless steel 441 in air with less than 3.5 vol. % H_2O was following quasi-parabolic mechanism. When the water vapor content

increased, the alloy was in "break away" oxidation. The oxidation rate of stainless steel samples increased with increasing time when the water vapor content was higher than 10 vol. %. Water vapor showed complex effects on the oxidation behavior of stainless steel.

The oxide scale structure of stainless steel 441 in water vapor containing atmosphere was different from that in dry air. Small content of water vapor promoted the sintering of oxide grains. It could be due to the transportation of Cr-containing vapor between the chromium oxide grains. With the existence of more water vapor, it would result in oxidative evaporation at high temperatures. At the same time, the sintering of the oxide grains was accelerated with the increasing water vapor content, which promoted the densification of the scale. This condition should be favorable toward resistance to further oxidation. Under this condition, the inward diffusion of oxygen, hydrogen and other particles could be more difficult than that in dry air atmosphere. As a result, the principal effect of water vapor on the parabolic oxidation process of the steel is likely to be the increase in diffusion resistance through the oxide scale in air with 3.5 vol. % H_2O.

On the other hand, higher Cr-containing vapor at water vapor containing atmosphere would cause dilution of Cr in the scales [25, 33]. Figure 10 shows the thermodynamic diagram of two dominant species of chromium volatilization. As the figure shows, CrO_3 is the main vapor product in the oxidation of Cr in dry air at high temperatures. When the atmosphere turns to be wet, $CrO(OH)_3$ becomes the main type of vapor. It can be found that the vapor pressures of CrO_3 and $CrO(OH)_3$ increase with enhancing oxygen partial pressure [18]. Based on the reported thermodynamic data [35, 36], the partial pressure of $CrO_2(OH)_2$ will exceed that of CrO_3 when the water vapor pressure is above about 10^{-2} atm at 1,000 °C in air. The total vapor pressure of the products in the oxidation process of stainless steel increases with the increasing content of water vapor in high temperature atmosphere. Thus, it could be concluded that water vapor could result in high Cr-containing vapor pressures in the oxidation of stainless steel, and $CrO_2(OH)_2$ could have a strong impact on the oxidation process at high water vapor content.

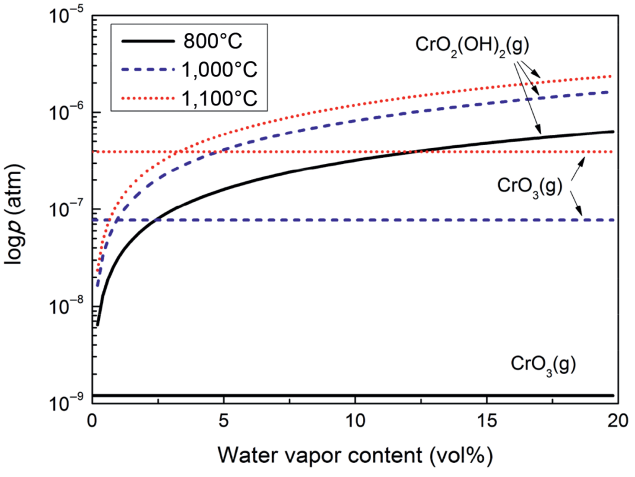

Figure 10: Equilibrium vapor pressures of CrO_3 and $CrO_2(OH)_2$ at 1,000 °C in air using thermodynamic data from [35, 36].

While, Fe-containing vapors also acts important role in the oxidation process of stainless steel at high temperature. The observed blade iron oxides on the "bubbles" could be the precipitate of Fe-containing vapors. The observations of earlier researchers are similar to the present results, *viz.* blade hematite grains were observed on the oxide layers of stainless steel [24, 37, 38], which could be attributed to the vapor of the products [39]. The loss of iron in iron-reached oxides layer resulted porous structure of it, which promoted the further break away oxidation of stainless steel.

Conclusion

(1) The oxidation rate of stainless steel 441 in wet air with 3.5 vol. % H_2O was found to be as low as that in dry air. Water vapor promoted the oxidation resistance of oxidized stainless steel due to the sintering of the oxide grains in low water vapor containing atmosphere.

(2) The oxidation process of stainless steel 441 in dry air followed quasi-parabolic model. The rate constants k_d and k_s were 2.09×10^{-5} and 4.51×10^{-6} mg·cm^{-2}·s^{-1}, respectively.

(3) In the oxidation process of stainless steel 441 in steam containing atmosphere, the growth stress of oxides scale increased relatively slowly, which increased to the maximum value within 70 ks. And a slow increasing content of Fe-containing spinel phase was found at the same time.

(4) The increasing water vapor content resulted in numbers of defects in the scale. This, in turn, promoted Fe- and Cr-containing species evaporation. The vapors compared the breakage of the chromium

oxide scale. Porous Fe-rich oxides layer developed from the "bubbles" and broken places, expanding on the scale, which caused the "break-away" oxidation of the steel in high water vapor containing atmosphere.

Funding: The authors gratefully thank the financial support of National Program on Key Basic Research Project of China (Grant No. 2012CB215405), China Postdoctoral Science Foundation (No. 2015M570036) and National Nature Science Foundation of China (No.51474141). The authors also thank Ms. Xiao-Jia Du for material supply.

References

[1] Y. Zhao and J. Fergus, J. Electrochem. Soc., 159 (2012) C109–C113.
[2] J. Wu and X. Liu, J. Mater. Sci. Technol., 26 (2010) 293–305.
[3] G. Meier, K. Jung, N. Mu, N. Yanar, F. Pettit, J. Pirón Abellán, T. Olszewski, H.L. Nieto, W.J. Quadakkers and G.R. Holcomb, Oxid. Met., 74 (2010) 319–340.
[4] R. Viswanathan, J. Sarver and J.M. Tanzosh, J. Mater. Eng. Perform., 15 (2006) 255–274.
[5] Y. Yamamoto, M.P. Brady, M.L. Santella, H. Bei, P.J. Maziasz and B.A. Pint, Metall. Mater. Trans. A., 42 (2011) 922–931.
[6] B.A. Pint, JOM., 65 (2013) 1024–1032.
[7] S.R.J. Saunders, M. Monteiro and F. Rizzo, Prog. Mater. Sci., 53 (2008) 775–837.
[8] M.P. Brady, M. Fayek, J.R. Keiser, H.M. Meyer Iii, K.L. More, L.M. Anovitz, D.J. Wesolowski and D.R. Cole, Corros. Sci., 53 (2011) 1633–1638.
[9] Y. Larring, R. Haugsrud and T. Norby, J. Electrochem. Soc., 150 (2003) B374–B379.
[10] J. Gong, Y.M. Jiang, B. Deng, C. Zhong, D.M. Sun and J. Li, Metall. Mater. Trans. A., 40 (2009) 2511–2513.
[11] E. Essuman, G. Meier, J. Żurek, M. Hänsel and W. Quadakkers, Oxid. Met., 69 (2008) 143–162.
[12] S. Henry, J. Mougin, Y. Wouters, J.-P. Petit and A. Galerie, Mater. High. Temp., 17 (2000) 231–235.
[13] N. Othman, J. Zhang and D. Young, Oxid. Met., 73 (2010) 337–352.
[14] H. Nickel, Y. Wouters, M. Thiele and W. Quadakkers, Fresenius J. Anal. Chem., 361 (1998) 540–544.
[15] J. Shen, L. Zhou and T. Li, Oxid. Met., 48 (1997) 347–356.
[16] W.J. Quadakkers, J. Żurek and M. Hänsel, JOM., 61 (2009) 44–50.
[17] H. Buscail, S. Heinze, P. Dufour and J.P. Larpin, Oxid. Met., 47 (1997) 445–464.
[18] J. Hammer, S. Laney, R. Jackson, K. Coyne, F. Pettit and G. Meier, Oxid. Met., 67 (2007) 1–38.
[19] L. Barelli, E. Barluzzi and G. Bidini, Int. J. Hydrogen Energy., 38 (2013) 5060–5074.
[20] M. Krumpelt, T.A. Cruse, B.J. Ingram, J.L. Routbort, S. Wang, P.A. Salvador and G. Chen, J. Electrochem. Soc., 157 (2010) B228–B233.
[21] J.J. Bentzen, J.V.T. HÃ¸gh, R. Barfod and A. Hagen, Fuel Cells., 9 (2009) 823–832.
[22] D. Young and B. Pint, Oxid. Met., 66 (2006) 137–153.
[23] Z. Yang, G. Xia, P. Singh and J.W. Stevenson, Solid State Ionics., 176 (2005) 1495–1503.
[24] F. Liu, J.E. Tang, H. Asteman, J.-E. Svensson, L.-G. Johansson and M. Halvarsson, Oxid. Met., 71 (2009) 77–105.
[25] H. Asteman, J.E. Svensson, M. Norell and L.G. Johansson, Oxid. Met., 54 (2000) 11–26.
[26] M. Halvarsson, J.E. Tang, H. Asteman, J.E. Svensson and L.G. Johansson, Corros. Sci., 48 (2006) 2014–2035.
[27] M. Hanesch, Geophys J. Int., 177 (2009) 941–948.
[28] J. Mougin, T. Le Bihan and G. Lucazeau, J. Phys. Chem. Solids., 62 (2001) 553–563.
[29] J. Mougin, N. Rosman, G. Lucazeau and A. Galerie, J. Raman Spectro., 32 (2001) 739–744.
[30] A. Srisrual, S. Coindeau, A. Galerie, J.P. Petit and Y. Wouters, Corros. Sci., 51 (2009) 562–568.
[31] A. Galerie, F. Toscan, M. Dupeux, J. Mougin, G. Lucazeau, C. Valot, A.M. Huntz and L. Antoni, Mater. Res., 7 (2004) 81–88.
[32] J. Mougin, A. Galerie, M. Dupeux, N. Rosman, G. Lucazeau, A.M. Huntz and L. Antoni, Mater. Corros., 53 (2002) 486–490.
[33] H. Asteman, J.E. Svensson and L.G. Johansson, Corros. Sci., 44 (2002) 2635.
[34] J.W. Fergus, Mater. Sci. Eng. A., 397 (2005) 271–283.
[35] Y.W. Kim and G.R. Belton, Metall. Trans., 5 (1974) 1811–1816.
[36] E.J. Opila, D.L. Myers, N.S. Jacobson, I.M.B. Nielsen, D.F. Johnson, J.K. Olminsky and M.D. Allendorf, J. Phys. Chem. A., 111 (2007) 1971–1980.
[37] B. Pujilaksono, T. Jonsson, H. Heidari, M. Halvarsson, J.E. Svensson and L.G. Johansson, Oxid. Met., 75 (2011) 183–207.
[38] G. Raynaud and R. Rapp, Oxid. Met., 21 (1984) 89–102.
[39] W.-K. Burton, N. Cabrera and F. Frank, Philos. Trans. Roy. Soc. London A., (1951) 299–358.